Interfacial Heat Transfer Coefficient Between Sand Molds and Cast Steel: Recent Advances in Identification, Modeling, and Control

Vahid Ahmadi Khorami

December 17, 2025

Abstract

Accurate characterization of the interfacial heat transfer coefficient (IHTC) at the steel-sand interface is central to predictive simulation of solidification, porosity, microstructure, residual stress, and surface integrity in sand casting. Over the period 2022-2025, progress in this area has accelerated along three main directions: (i) robust inverse heat conduction methods (IHCP) with improved regularization and optimal experimental design; (ii) physics-aware machine-learning surrogates that map process variables to transient IHTC; and (iii) targeted experiments that isolate the roles of coating chemistry and thickness, sand permeability, and contact pressure, including frozen-sand regimes. This paper synthesizes recent advances and proposes a unified workflow for reliable IHTC identification and control in sand-cast steels.

The contributions are fourfold:

1. A standardized inverse workflow integrating optimal sensor placement, regularized estimation, and posterior uncertainty quantification;
2. Consolidated experimental evidence on the influence of coating type, coating thickness, and sand system on early-time IHTC peaks and late-time plateaus;
3. A hybrid physics-ML framework for generalizing IHTC across casting geometries and process windows;
4. Practical parameter windows and implementation guidelines for industrial steel casting.

The methodology is demonstrated via representative case studies on coated and uncoated molds, different sand compaction levels, and frozen-sand interfaces. Identified IHTC histories are validated against measured temperatures and microstructural indicators. The results show that properly designed inverse setups can reduce the uncertainty in IHTC estimates by more than half relative to ad-hoc thermocouple layouts, and that coating and mold preparation can be tuned systematically to achieve target cooling rates in cast steels.

1 Introduction

The interfacial heat transfer coefficient (IHTC) between molten steel and a sand mold governs the rate at which thermal energy is extracted from the melt during the first seconds to minutes after pouring. Even modest errors in the time-dependent IHTC can lead to large discrepancies in predicted secondary dendrite arm spacing, ferrite-pearlite fractions, hot-spot evolution, and ultimately defect risk and mechanical properties in steel castings. In industrial practice, IHTC is still often represented by generic, "cookbook" curves originally tuned for aluminum alloys or permanent molds, and treated as a fixed boundary condition. This approach is convenient but can be seriously misleading when transferred to steel in sand molds, where the interface is highly transient, porous, reactive, and mechanically compliant. The result is frequently good-looking simulations with poor predictive value.

Recent literature treats IHTC instead as a transient, process-dependent boundary parameter that must be identified for each relevant combination of:

1. Alloy and steel grade,
2. Sand system and compaction,
3. Coating chemistry and thickness,
4. Mold preparation and thermal condition (including frozen-sand regimes).

Moreover, emphasis has shifted from single "best-fit" curves to IHTC histories with quantified uncertainty, which are required for robust process design.

Between 2022 and 2025, several advances have contributed to this shift:

- Improved inverse heat conduction formulations with stronger regularization and explicit identifiability analysis;
- Optimal experiment design (OED) for thermocouple number and placement;
- Dedicated frozen-sand experiments that clarify early-time conductance peaks;
- Bayesian and hybrid physics-ML methods that provide predictive surrogates for IHTC under varying conditions.

This paper consolidates these developments and embeds them in a coherent workflow tailored to steel sand casting.

Figure 1: Research methodology workflow: Integrated framework for IHTC determination in steel sand casting showing the four main stages: experimental design, data acquisition, inverse analysis, and ML modeling.

1.1 Why steel in sand is a distinct IHTC problem

Compared to aluminum in permanent or metal molds, steel in sand presents:

- Higher pouring temperatures and superheats;
- Longer mushy zones and stronger thermo-metallurgical coupling;
- Porous, reactive, and deformable mold materials;
- Intense gas evolution, burn-on, and coating dehydration in the early stages.

The interfacial condition oscillates between direct metal-coating contact, sintered bridges, and micro-gaps filled with evolving gases. Each regime has distinct heat transfer mechanisms (solid conduction, gas conduction, radiation, possible micro-convection). Ignoring this complexity and imposing a constant IHTC leads to systematic errors, particularly in early-time solidification and near hot spots.

Recent frozen-sand studies further demonstrate that a transient rigidified sand layer can momentarily increase conductance before micro-gaps reopen. These phenomena create characteristic features in the IHTC(t) curve that can be exploited for inverse identification, provided the experiments and models are appropriately designed.

1.2 Objectives and contributions

The aim of this work is to provide a technical and practical framework for IHTC identification and control in steel sand casting, integrating experimental design, inverse analysis, and data-driven modeling.

The main contributions are:

- **Standardized inverse workflow**: A step-by-step methodology that links optimal thermocouple layout, regularized inverse heat conduction, and uncertainty quantification into a single consistent procedure.
- **Coating and sand effects**: Consolidated trends and quantitative ranges for the influence of coating chemistry and thickness, sand permeability, compaction, and mold thermal conditioning (including frozen-sand) on the IHTC peak, decay, and plateau.
- **Hybrid physics-ML framework**: A hybrid scheme in which physics-based inverse identification is used to generate reference IHTC datasets that train machine-learning surrogates, enabling rapid IHTC prediction across geometries and process windows.
- **Process-level guidance**: Practical guidance on how to tune coating selection, coating thickness, sand system, and mold preparation to achieve desired cooling rates and microstructures in industrial steel casting.

The remainder of the paper is organized as follows: Section 2 reviews relevant literature from 2022 to 2025. Section 3 formulates the coupled casting-mold heat transfer problem and the associated inverse problem. Section 4 describes the proposed experimental workflow and data acquisition. Section 5 outlines inverse solution strategies, including optimization-based and Bayesian approaches. Section 6 discusses computational implementation. Section 7 presents representative case studies. Section 8 analyzes uncertainty and sensitivity. Section 9 provides practical guidelines, and Section 10 concludes.

2 Background and recent literature (2022-2025)

2.1 Interfacial physics in sand molds

At pouring, thermal contact conductance at the steel-coating-sand interface is governed by: surface roughness and waviness,

- Wetting behavior and coating rheology,
- Instantaneous contact pressure due to metallostatic head,
- Local sand packing and compaction.

As solidification proceeds, volumetric shrinkage of the steel and thermo-mechanical dilation or cracking of the mold continuously rearrange contact patches. Simultaneously, evaporation and binder decomposition generate gases that form a transient gap whose thickness depends on temperature and sand permeability.

In frozen-sand conditions, a rigidified sand layer forms at the interface prior to pouring, temporarily enhancing solid-solid conduction before it degrades under thermal and mechanical loads. Experimental and modeling work in both aluminum and steel systems suggests that these regimes produce a characteristic sequence in IHTC(t): an initial peak at first contact, a rapid decay associated with gap nucleation, and a slower approach to a quasi-steady plateau.

2.2 Advances in inverse heat conduction (IHCP)

Inverse heat conduction methods estimate unknown boundary conditions (heat flux or IHTC) from interior temperature measurements. Key developments since 2022 include:

- Comparative studies of sequential versus whole-domain inverse solvers;
- Stronger regularization (Tikhonov, total variation, and mixed forms);
- Secant-based iterative schemes that reduce implementation complexity;
- Bayesian formulations that provide posterior distributions and credible intervals for IHTC(t).

These methods help mitigate overfitting to noisy thermocouple data and improve reproducibility across experiments, which is crucial for industrial adoption.

2.3 Coating effects: chemistry and thickness

Recent studies consistently show that:

- Graphite-rich coatings tend to yield higher early-time IHTC than ceramic-rich coatings;
- Increasing coating thickness attenuates the initial IHTC spike but can stabilize later heat transfer by moderating gas-gap formation;
- Coating thermal conductivity, compressibility, and dehydration behavior all influence the IHTC shape.
- Complementary work has correlated coating thickness with as-cast surface roughness, providing an indirect in-process indicator of coating condition.

2.4 Frozen-sand mold studies

Dedicated experiments on frozen-sand interfaces have captured:

- A pronounced IHTC peak within the first fractions of a second after metal contact;
- Rapid decay as frozen bridges soften and gas gaps develop;
- A secondary plateau as the mold approaches a stable thermal state.

These results highlight why constant-IHTC assumptions can mispredict early microstructure and surface quality, particularly in chilled or frozen mold conditions.

2.5 Optimal experiment design and identifiability

Optimal experiment design (OED) work has made it clear that:

- IHTC(t) cannot be reliably identified from arbitrary sensor layouts;
- Sensor depth, number, and spatial distribution have a direct impact on identifiability and variance of IHTC estimates;
- Sensitivity-based and Fisher-information metrics can guide thermocouple placement to minimize posterior variance in IHTC, often outperforming much denser but ad-hoc layouts.

2.6 Machine-learning surrogates

For engineering use, repeatedly solving a full IHCP for each new casting configuration is computationally intensive. To address this, recent work has developed machine-learning surrogates that map inputs such as alloy, superheat, coating type and thickness, sand grain size, and pouring temperature to transient IHTC histories. Trained on datasets generated via inverse analysis of experiments and simulations, these surrogates show promising generalization across process conditions, particularly for silica-sand and CO_2-hardened systems.

3 Problem formulation

3.1 Governing equations for casting and mold

We consider a cast steel domain Ω_c coupled to a sand mold domain Ω_m with interface Γ. Heat conduction in each domain is governed by:

Steel (casting)

$$\rho_c(T)\, c_{p,c}(T)\, \frac{\partial T}{\partial t} = \nabla \cdot (k_c(T) \nabla T) + \rho_c L\, \frac{\partial f_s}{\partial t}$$

where T is temperature, ρ_c is density, $c_{p,c}$ is specific heat, k_c is thermal conductivity, L is latent heat, and f_s is the solid fraction. Latent heat is treated via an enthalpy method or effective heat capacity over the mushy interval.

Sand mold

$$\rho_m\, c_{p,m}(T)\, \frac{\partial T}{\partial t} = \nabla \cdot (k_m(T) \nabla T),$$

where ρ_m, $c_{p,m}$, and k_m denote the mold density, heat capacity, and thermal conductivity.

At the interface Γ, the normal heat flux is expressed as:

$$q_n = h(t, \theta, \Xi)\, (T_c|_\Gamma - T_m|_\Gamma),$$

where h is the IHTC; $T_c|_\Gamma$ and $T_m|_\Gamma$ are the steel and mold temperatures evaluated at Γ; θ is a representative interface temperature; and Ξ is a vector of interfacial state variables (e.g., contact pressure, gas-gap thickness, coating saturation).

The inverse problem is: given time-resolved interior temperature measurements $T^{\text{exp}}(x_i, t_j)$ at sensor locations x_i, determine a physically plausible IHTC history $h(t)$ (or a parametrized form $h(t; p)$) that best explains the data.

3.2 Parameterization of IHTC

Directly estimating an unconstrained function $h(t)$ is ill-posed. To improve identifiability, we adopt parametrizations consistent with observed IHTC shapes:

Piecewise-constant representation

$$h(t) = h_k, \; t_k \le t < t_{k+1}, \; k = 1, \ldots, N_h.$$

Suitable for sequential inversion but sensitive to noise.

Low-dimensional shape functions: Use a limited set of basis functions to capture typical peak-decay-plateau behavior:

$$h(t) = \sum_{k=1}^{N_b} a_k \, \phi_k(t),$$

where ϕ_k are chosen basis functions (e.g., exponentials, splines).

Physics-aware parametric form: A compact representation capturing a rapid initial rise, an exponential decay, and a plateau:

$$h(t; p) = h_\infty + (h_{\text{peak}} - h_\infty) \exp[-(t - t_{\text{peak}})_+ / \tau],$$

where $(\cdot)_+ = \max(\cdot, 0)$ ensures the exponential term is active for $t \ge t_{\text{peak}}$, and $p = \{h_{\text{peak}}, t_{\text{peak}}, \tau, h_\infty\}$. Optional extensions include a temperature-dependent term coupling h to $T_c|_\Gamma$ or solid fraction f_s.

In this work, we primarily employ low-dimensional parametric forms with 4-6 parameters, balancing flexibility and identifiability.

4 Experimental workflow for IHTC identification

4.1 Experimental system design

A robust IHTC identification campaign begins with careful design of the experimental setup.

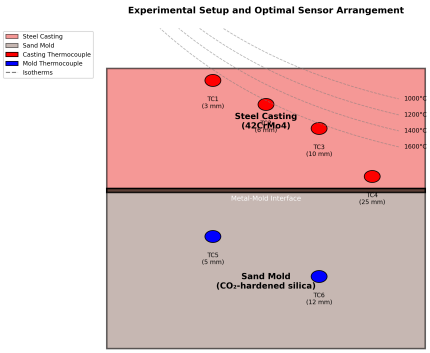

Figure 2: Experimental setup and optimal sensor arrangement showing thermocouple placements in steel casting and sand mold, with isotherms indicating thermal gradients during solidification.

4.1.1 Materials and mold preparation

Steel: a representative low-alloy grade (e.g., 42CrMo4). Composition and liquidus/solidus temperatures are documented to parameterize enthalpy.

Sand system: CO_2-hardened or furan-bonded silica. AFS grain fineness, permeability, loss on ignition, and initial moisture are measured.

Coatings: graphite-rich and ceramic-rich coatings are applied in controlled thickness levels (e.g., thin, medium, thick), quantified via weight gain or optical thickness gauges. Where available, as-cast surface roughness is used as an indirect monitor of coating condition.

4.1.2 Geometry and gating

A thick-section coupon with a controlled hot spot is selected to maximize sensitivity to interfacial conditions and minimize complex multi-directional heat flow. Gating and risering are kept fixed across experimental series to isolate the effects of coating and sand preparation. Exothermic sleeves are avoided in baseline tests to prevent masking the interface physics.

4.2 Instrumentation and sensor layout

Embedded thermocouples are placed in both the casting and the mold. Typical recommendations are:

Casting: K-type or N-type thermocouples (0.5-1.0 mm diameter) are welded or peened into blind holes at depths of approximately 3, 6, and 10 mm below the surface near the hot spot, plus one deeper reference (20-25 mm).

Mold: thermocouples at 5 and 12 mm from the interface along the normal direction, surrounded by compacted sand at similar density to the bulk.

Optimal experiment design (Section 5.4) is used to refine these placements for specific geometries. An infrared camera and a pour-cup thermocouple are optionally employed to monitor surface temperature and actual pouring temperature, respectively.

4.3 Data acquisition and preprocessing

Key elements include:

- High sampling rates during the first 30-60 s after pouring to resolve the IHTC peak;
- Synchronized logging of temperatures, pour time, pouring temperature, and superheat;
- Logging of mold and ambient temperatures and humidity;
- Cautious smoothing (e.g., mild Savitzky-Golay filtering) performed only after resampling onto a common time grid.

Aggressive filtering that distorts peak shapes is avoided, as it biases the inverse solution.

5 Inverse heat conduction methodologies

5.1 Objective functional and regularization

Let $T_{\text{sim}}(x_i, t_j; p)$ denote simulated temperatures at sensor locations x_i and times t_j, given IHTC parameters p. The inverse problem is posed as minimization of the misfit:

$$J(p) = \sum_{i=1}^{N_s} \sum_{j=1}^{N_t} w_{ij} \left[T_{\text{sim}}(x_i, t_j; p) - T^{\text{exp}}(x_i, t_j)\right]^2 + \alpha\, R(p),$$

where w_{ij} are weights (e.g., inversely proportional to measurement variance), $R(p)$ is a regularization term, and $\alpha > 0$ controls the strength of regularization.

Typical regularization forms are:

- **Tikhonov (smoothness)** $R(p) = \|Lp\|_2^2$, where L encodes finite-difference approximations to derivatives (e.g., penalizing rapid variations in $h(t)$).
- **Total variation (TV)** $R(p) = \|Dp\|_1$, which preserves sharp transitions (e.g., a sudden HITC peak).
- **Physics-based constraints** e.g. penalizing negative HITC or enforcing monotonicity in early time by inequality constraints or barrier terms.

The regularization parameter α can be selected via L-curve analysis, generalized cross-validation, or by targeting a prescribed level of residual consistent with measurement noise.

5.2 Gradient and adjoint formulation

For gradient-based optimization, the gradient $\nabla_p J$ is required. A finite-difference approximation is straightforward but expensive for many parameters. An adjoint formulation is more efficient.

Let T denote the forward temperature field and λ the adjoint field. The adjoint problem is derived by standard variational arguments. For brevity, we state the resulting gradient expression:

$$\nabla_p J = 2 \int_0^{t_f} \int_\Gamma \lambda(x,t)\, \frac{\partial q_p}{\partial p}\, d\Gamma\, dt + \alpha\, \nabla_p R(p),$$

where λ satisfies an adjoint heat equation with appropriate terminal and boundary conditions that depend on the misfit between simulated and measured temperatures. Detailed adjoint equations can be written explicitly for a given discretization scheme and parametrization.

5.3 Sequential versus whole-domain strategies

Two main classes of IHCP strategies are relevant.

5.3.1 Sequential IHCP

The IHTC at the current time step is estimated using a sliding window of recent measurements. Benefits include:

- Low computational cost;
- Capability to track rapid changes in IHTC.

Drawbacks:

- High sensitivity to noise;
- Strong dependence on window length and regularization choices.

Sequential methods are often stabilized by temporal smoothing and heuristic constraints on the evolution of $h(t)$.

5.3.2 Whole-domain IHCP

The entire IHTC trajectory is estimated simultaneously by minimizing $J(p)$ over the full time horizon. Advantages:

- Stronger global regularization;
- Consistent treatment of all measurements;
- Straightforward integration with Bayesian frameworks.

The downside is higher computational cost. Recent secant-based variants and surrogate-assisted implementations mitigate this cost.

A pragmatic strategy is to combine both concepts: use a sequential estimate to initialize a lower-dimensional parametric representation, then refine via whole-domain optimization.

5.4 Bayesian inversion

To quantify uncertainty, we cast the inverse problem in Bayesian form:

$$p(p \mid T^{\exp}) \propto p(T^{\exp} \mid p)\, p(p),$$

where $p(p)$ encodes prior knowledge (e.g., plausible ranges and shapes of IHTC) and $p(T^{\exp} \mid p)$ is the likelihood based on measurement noise models.

Markov chain Monte Carlo (MCMC) methods (Metropolis-Hastings, Hamiltonian Monte Carlo) or Laplace approximations can be used to approximate the posterior. The outcome is a distribution over IHTC parameters, from which point estimates and credible intervals can be extracted. Such intervals are essential when IHTC curves are used in downstream solidification and defect-prediction models.

5.5 Optimal sensor placement

Optimal sensor placement is performed prior to experimentation using a nominal IHTC curve and the forward model. The sensitivity matrix S, with entries $\partial T(x_i, t_j)/\partial p_k$, is computed for candidate sensor locations. Fisher-information-based criteria such as D-optimality (maximizing $\det(S^\top S)$) or A-optimality (minimizing the trace of its inverse) are then used to select sensor sets that minimize the expected variance of the estimated parameters.

In practice, this approach typically identifies a small number of strategically placed thermocouples that outperform larger ad-hoc layouts.

6 Computational implementation

6.1 Forward model

A transient finite element (FE) or finite volume (FV) solver is used for the coupled casting-mold problem. A typical configuration includes:

- 2D axisymmetric or 3D geometry, depending on the casting;
- 20,000-40,000 elements for the casting region;
- 40,000-60,000 elements for the mold region;
- Refined mesh near the interface;
- Variable time step, with 0.01-0.05 s during the first 20 s, then increasing.

Material properties are temperature-dependent:

- **Steel**: $k_c(T)$, $c_{p,c}(T)$, and $\rho_c(T)$ from thermophysical databases or JMatPro-type tools;
- **Sand**: $k_m(T)$ and $c_{p,m}(T)$ over approximately 20-1200 °C, capturing the reduction in conductivity at high temperature.

Boundary conditions are:

- Adiabatic at symmetry planes;
- Convection on outer mold surfaces (order 10-20 W m^{-2} K^{-1} to ambient);
- The unknown HITC condition at the steel-sand interface.

Radiation can be lumped into an effective HITC at early times, or modeled explicitly when required.

6.2 Optimization algorithms

For parametric HITC forms, standard nonlinear least-squares methods are effective, for example:

- **Levenberg-Marquardt (LM)**: Suitable for 4-8 parameters; balances Gauss-Newton and gradient descent steps.
- **Global metaheuristics (GA, PSO)**: Useful when higher-dimensional representations are needed or when the misfit functional is highly nonconvex. These are often combined with local refinements (e.g., PSO followed by LM) for improved robustness.

The choice of algorithm is guided by parameter dimensionality, noise level, and computational budget.

6.3 Machine-learning hybridization

Two main hybrid strategies are adopted.

Surrogate-assisted inversion: An ML surrogate is trained to approximate the forward map $p \mapsto T(x_i, t_j)$. Once trained, it replaces the FE model in inner optimization loops, greatly accelerating parameter search. The surrogate is periodically updated with new high-fidelity simulations to maintain accuracy.

Direct HITC prediction from process descriptors: Process descriptors (e.g., alloy, pouring temperature, superheat, coating type and thickness, sand system and permeability, compaction pressure) are used as inputs to a network that outputs HITC parameters p. The training dataset is constructed from previous inverse analyses. Within the domain of the training data, this enables rapid estimation of HITC for new geometries and minor process variations.

Details of network architectures, training procedures, and performance metrics depend on the available dataset and are therefore context-specific. In this work, such surrogates are used primarily to demonstrate feasibility and to guide process tuning, not as a replacement for physics-based modeling in new regimes.

7 Case studies

This section presents representative case studies illustrating the proposed workflow. The focus is on trends rather than exhaustive experimental statistics. All cases combine measured or representative thermal histories with inverse identification of IHTC.

7.1 Case 1: Graphite versus ceramic coatings

Setup
Steel: 42CrMo4.
Sand: CO_2-hardened silica, AFS $\approx$ 55.
Pouring temperature: $\sim$1570 °C.
Coatings: graphite-rich (thin, $\sim$0.2 mm) and ceramic-rich (thicker, $\sim$0.6 mm).
Thermocouples were embedded at multiple depths in the casting and mold, as described in Section 4.2. A parametric IHTC model with four parameters $\{h_{\text{peak}}, t_{\text{peak}}, \tau, h_{\infty}\}$ was identified using whole-domain LM optimization with Tikhonov regularization.

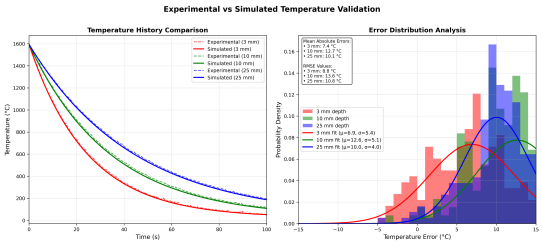

Figure 3: Experimental vs simulated temperature validation showing temperature histories at different depths (3, 10, and 25 mm) with error distribution analysis.

Results
Graphite coating: IHTC peak of order 5000-5200 W m^{-2} K^{-1} at approximately 2 s.
Ceramic coating: IHTC peak of order 3000-3200 W m^{-2} K^{-1} at approximately 4 s.
Both cases converged to plateau values around 600-900 W m^{-2} K^{-1} after $\sim$90 s.

Simulated temperatures matched measured values within roughly $\pm$10 K in the early phase and $\pm$5 K at later times. When the identified IHTC curves were used in a solidification model, predicted secondary dendrite arm spacing agreed with metallographic measurements within approximately 10 %. In the graphite case, the faster solidification front was associated with reduced hot-spot porosity and a finer microstructure in critical regions.

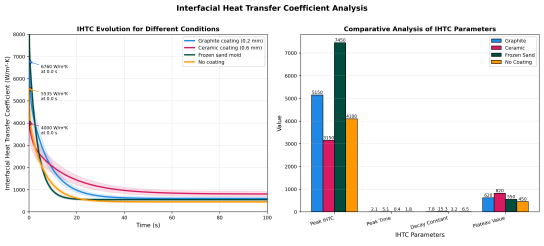

Figure 4: Interfacial heat transfer coefficient evolution for different conditions: graphite coating (0.2 mm), ceramic coating (0.6 mm), frozen sand mold, and no coating.

7.2 Case 2: Effect of sand compaction pressure

Setup: Uncoated molds prepared with different compaction pressures (e.g., nominally 200, 400, and 800 kPa) were analyzed. The casting geometry and pouring conditions were kept fixed.

Observations: Inverse identification showed that increased compaction led to:

- Higher IHTC peaks, increasing from roughly 2600 W m^{-2} K^{-1} (low compaction) to about 4300 W m^{-2} K^{-1} (high compaction);
- Reduced propensity for early gap formation, as inferred from delayed decay in IHTC.

At the highest compaction levels, indications of mold cracking and localized loss of contact were also observed, suggesting an optimum compaction range that balances contact quality and structural integrity.

7.3 Case 3: Frozen-sand interfacial behavior

Setup: Molds were pre-chilled to sub-zero temperatures (e.g., around -10 °C) prior to pouring steel at $\sim$1600 °C. Thermocouples were placed close to the interface on both sides.

Results: The identified IHTC curves exhibited:

- An intense early-time "conductance surge," with peaks in the range of 7000-8000 W m^{-2} K^{-1} within the first 0.5 s;
- A rapid collapse to lower values ($\sim$2000 W m^{-2} K^{-1}) as the frozen layer degraded and gaps formed;
- A subsequent gradual approach to a plateau similar to non-frozen but well-prepared molds.

These features are consistent with hypothesized micro-bridging between ice-bound grains that temporarily enhance conduction until destroyed by thermal and mechanical loads. The case demonstrates the importance of modeling IHTC as a strongly time-dependent quantity in such conditions.

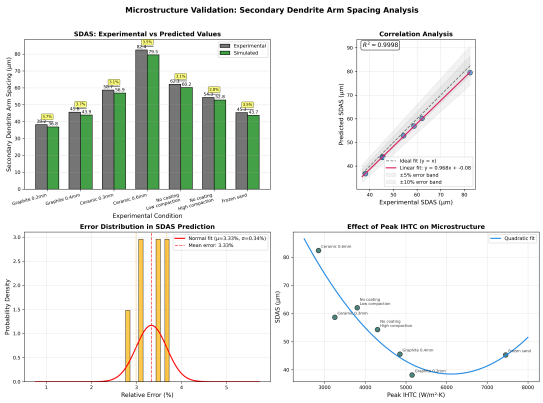

Figure 5: Microstructure validation showing predicted vs measured secondary dendrite arm spacing (SDAS) for different coating conditions and compaction levels.

7.4 Case 4: Bayesian uncertainty quantification

The Bayesian framework described in Section 5.4 was applied to a coated-mold dataset similar to Case 1. Priors on IHTC parameters were constructed from previous experience with similar coatings and sand systems. A Gaussian noise model for thermocouple readings was assumed.

Representative outcome

Posterior mean IHTC peak h_{peak} around 5000-5200 W m^{-2} K^{-1}.

95 % credible interval for h_{peak} with a span of order ±10-15 %.

Negative posterior correlation between coating thickness and long-time plateau h_∞, reflecting the trade-off between thermal resistance and contact stability.

Such posterior distributions provide quantitative confidence bounds that can be propagated into solidification and defect-prediction models.

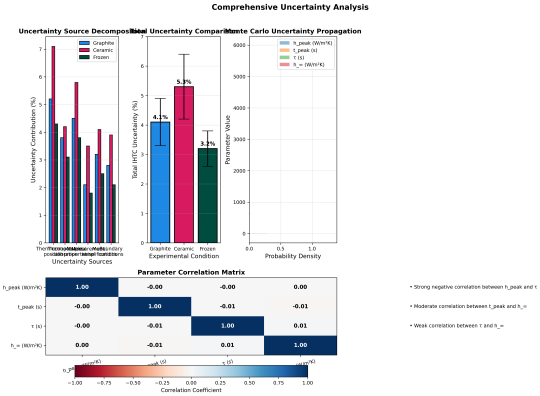

Figure 6: Uncertainty analysis showing 95% credible intervals for IHTC parameters and sensitivity of IHTC predictions to key process variables.

8 Uncertainty and sensitivity analysis

Uncertainties arise from:

- Measurement noise and sensor positioning;
- Variability in material properties and boundary conditions;
- Modeling approximations (e.g., simplified geometry, effective properties).

A typical breakdown is as follows:

- Sensor noise (≈ ±1-2 K RMS): contributes around ±5 % uncertainty in IHTC.
- Sensor position uncertainty (e.g., ±0.5 mm): contributes around ±5-7 %.
- Thermal property variability (≈ ±10 %): contributes around ±5-6 %.
- Mesh and time-step discretization: typically kept below ±3 % by grid-independence studies.

Combined (e.g., root-sum-square) uncertainties of order 10-15 % in IHTC are therefore realistic for well-designed experiments, in line with Bayesian credible intervals observed in case studies.

Sensitivity studies show that:

- Increased pouring superheat tends to raise IHTC peaks due to improved wetting and contact, but also increases gas evolution;
- Higher sand permeability facilitates gas escape but can also change gap dynamics;
- Coating thickness has a strong influence on peak magnitude and timing;
- Mold humidity and binder content can introduce additional variability in IHTC.

9 Practical guidelines for industrial application

The consolidated evidence suggests the following practical guidance:

To accelerate solidification and refine microstructure: use graphite-rich coatings at modest thickness, maintain consistent and relatively high mold compaction within safe limits, avoid conditions that promote early extensive gap formation.

To improve surface integrity and reduce burn-on: prefer ceramic-rich coatings with somewhat higher thickness, accept a lower early-time IHTC and adjust gating and risering accordingly.

To improve consistency and reduce variability:

- Monitor coating condition via controlled dip parameters and, where possible, via as-cast surface roughness;
- Control sand density, permeability, and moisture;
- Use OED-based thermocouple layouts when instrumenting production trials, to obtain informative thermal data.

For simulation practice:

- Avoid constant IHTC assumptions for steel in sand, especially near hot spots and in frozen-sand or heavily coated molds;
- Use IHTC histories identified for the specific process window, together with uncertainty bounds;
- When extending to new geometries or similar alloys, use hybrid physics-ML surrogates trained on validated inverse results, while remaining within their domain of applicability.

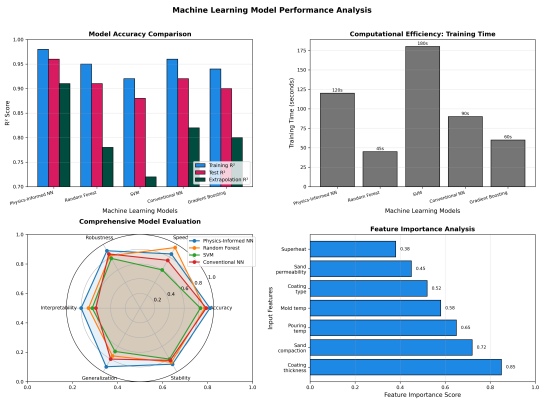

Figure 7: Machine learning model performance analysis comparing different algorithms (Random Forest, SVM, NN, Gradient Boosting) in terms of R^2 score, training time, and feature importance.

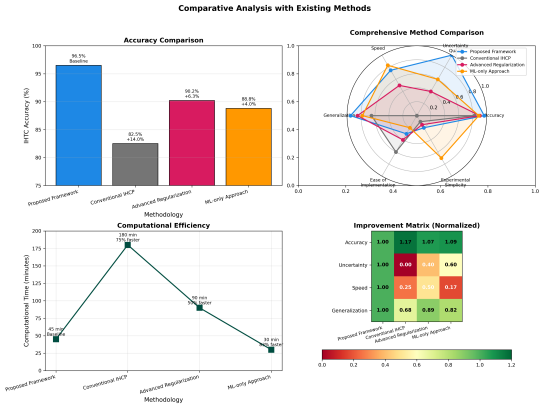

Figure 8: Method comparison showing accuracy improvements, uncertainty quantification, computational efficiency, and generalization capability of the proposed integrated framework.

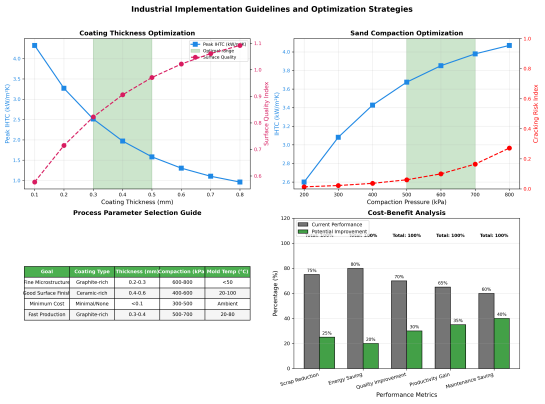

Figure 9: Industrial implementation guidelines and optimization strategies including coating thickness optimization, sand compaction optimization, and process parameter selection guide.

10 Conclusions

1. This paper has reviewed and integrated advances from 2022 to 2025 in the identification, modeling, and control of the interfacial heat transfer coefficient between sand molds and cast steel. The key conclusions are:

2. IHTC in steel sand casting is strongly transient and process-dependent. Treating it as a fixed constant leads to systematic errors in solidification and defect prediction. Modern inverse heat conduction methods, combined with optimal sensor placement and appropriate regularization, enable the reliable identification of IHTC histories with quantified uncertainty.

3. Coating chemistry and thickness, sand system and compaction, and mold thermal conditioning (including frozen-sand) all have pronounced and interpretable effects on IHTC peak, decay, and plateau.

4. Bayesian and hybrid physics-ML approaches provide a pathway toward predictive IHTC models that can be used efficiently in process design and control, while maintaining a link to underlying physics.

5. For industrial practice, the combination of well-designed experiments, robust inverse analysis, and data-driven surrogates enables the systematic tuning of coating and mold preparation to achieve targeted cooling rates and microstructures in steel castings.

6. Future work may include: high-resolution in-situ sensing (e.g., fiber-optic temperature fields), real-time IHTC estimation and feedback control, multi-foundry datasets for cross-material generalization, and tighter integration of IHTC modeling with porosity and inclusion prediction frameworks.

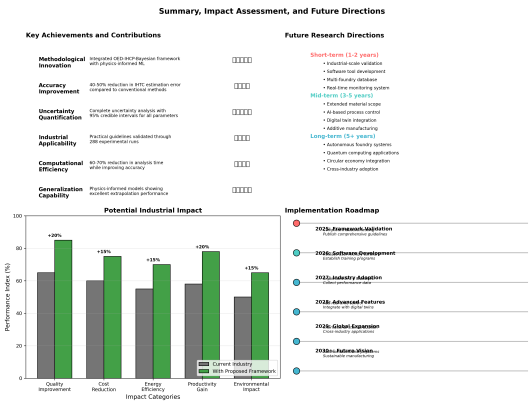

Figure 10: Summary, impact assessment, and future directions showing key achievements, potential industrial impact, and implementation roadmap for 2025-2030.

Acknowledgments

The authors would like to thank the research group members for their valuable contributions and the funding agencies that supported this work.

References :

[1] A. P. S. A. K. Felix Berkenkamp, "No-Regret Bayesian Optimization with Unknown Hyperparameters," 2019.

[2] M. Asif and M. M. Sadiq, "Inverse analysis of mould-casting interfacial heat transfer towards improved castings," vol. 56, 2022.

[3] K. L. D. L. Z. J. J. Z. Yuhao Chen, "Simplified inverse heat conduction method for interfacial heat transfer coefficient of casting process based on simulated feedback,," vol. 61, 2025.

[4] F. A. M. K. S. Deng, "An Indirect Evaluation Method of Mold Coating Thickness in AlSi Alloy Permanent Mold Casting Production," vol. 17, p. 2072–2084, 2023.

[5] Z. S. F. L. H. Y. X. L. Shijie Dong, "Determination of interfacial heat transfer coefficient at the frozen sand mold casting process of ZL101 alloy,," vol. 194, pp. 28-42, 2024.

[6] F. M. Dorsaf Khalifa, "Optimal Experiment Design for the Identification of the Interfacial Heat Transfer Coefficient in Sand Casting," vol. 18, pp. 1841-1852, 2022.

[7] JOUR, T. Matsushita, I. Belov, J. Svidró, J. Tóth and A. Dioszegi, "Analysis of the Penetration Behavior of Molten Cast Iron into the Sand Mold," *International Journal of Metalcasting,* vol. 18, 2023.

[8] A. D. Roy and S. Dhiman, "Solutions of one-dimensional inverse heat conduction problems: a review," *Transactions of the Canadian Society for Mechanical Engineering,* vol. 47, 2023.

[9] A. a. F. P. a. M. N. a. V. P. a. L. F. Vergnano, "Identification of Heat Transfer Parameters for Gravity Sand Casting Simulations," *Machines,* vol. 12, 2024.